We are IntechOpen,
the world's leading publisher of
Open Access books
Built by scientists, for scientists

6,900
Open access books available

186,000
International authors and editors

200M
Downloads

154
Countries delivered to

Our authors are among the

TOP 1%
most cited scientists

12.2%
Contributors from top 500 universities

WEB OF SCIENCE™

Selection of our books indexed in the Book Citation Index
in Web of Science™ Core Collection (BKCI)

Interested in publishing with us?
Contact book.department@intechopen.com

Numbers displayed above are based on latest data collected.
For more information visit www.intechopen.com

Phase and Polarization Contrast Methods by Use of Digital Holographic Microscopy: Applications to Different Types of Biological Samples

Francisco Palacios, Oneida Font, Guillermo Palacios, Jorge Ricardo, Miriela Escobedo, Ligia Ferreira Gomes, Isis Vasconcelos, Mikiya Muramatsu, Diogo Soga, Aline Prado and Valin José

1. Introduction

The light that crosses a biological material can contains phase (refractive), amplitude (absorption) and optical activity (state of polarization) information about the material itself. Bright-field microscopy is an invaluable tool for observation of biological material, and microscopists utilize the intensity data either naturally present in the sample or introduced by staining. Differential staining is a complex process enabling certain structures to be distinguished from others, yet staining is not always appropriate for living cells, or for materials that do not absorb the stain. In these cases, phase contrast microscopy is necessary.

Several methods are available to render phase structure visible. Among the numerous modalities of contrast enhancing techniques that have been developed for non-invasive visualization of unstained transparent specimens, phase contrast (PhC), initially proposed by Zernike as a means of image contrast method (Zernike, 1942a,1942b) as well as Nomarski's differential interference contrast (DIC) (Nomarski, 1955), are available for high-resolution light microscopy (Pluta, 1988) and are widely used in biology. These two contrast techniques allow transforming phase information into amplitude or intensity modulation, which can be detected by photosensitive media. Unlike the PhC and DIC microscopy techniques, interferometric

techniques present the great advantage of yielding quantitative measurements of parameters, including the phase distribution produced by transparent specimens.

Digital holography (DH) has several features that make it an interesting alternative to conventional microscopy. These features include an improved focal depth, possibility to generate 3D images and phase contrast images (Buraga-Lefebre et al., 2000; Seebacher et al., 2001; Xu et al., 2001). The technique of DH has been implemented in a configuration of an optical microscope (Schilling et al., 1997). The objective lens produces a magnified image of the object and the interference between this image and the reference beam is achieved by the integration of the microscope to one of the arms of a Mach–Zender interferometer. The interference pattern is recorded by a digital camera. This configuration is called Digital Holographic Microscopy (DHM).

DHM has been demonstrated in many applications as in observation of biological samples (Popescu et al., 2004; Palacios et al., 2005; Kim, 2010, Ricardo et al., 2011), living cells analysis (Carl, 2004; Kemper et al., 2006) and cell death detection (Pavillon et al., 2012) because most biological samples are phase objects. Emery (Emery et al., 2007) applied DHM to dynamic investigation of natural and stimulated morphological changes associated with chemical, electrical or thermal stimulation. Hu (Hu et al., 2011), performed a quantitative research with gastric cancer cells in different periods of cell division under marker-free condition in real-time. DHM technique also allows implementing processing methods to perform phase contrast imaging (Cuche et al., 1999), besides possessing unique advantages as non-destructive and non-invasive analysis.

DH with an off-axis configuration has also been applied for polarization imaging by using orthogonally polarized reference waves (Colomb et al., 2002; Colomb et al., 2004). The advantages of DH over the other polarimetries are its relatively simple optical system without any rotating optics and its adaptability to three dimensional objects due to numerical focusing (Nomura et al., 2007). Polarization microscopy can reveal inner structures of cells without the need of contrast agents, and it is possible to give access to intrinsic information about their morphology and dynamics through the phase change quantification in these microscopic structures. An associated technique which uses the phase information for studying the state of polarization of live neurons in culture was developed by (Wang et al., 2008). However, according to recent publications, the Holographic Microscopy for polarization imaging (Polarization Holographic Microscopy, PHM), has been poorly applied to biological specimens analysis but only to fiber optics (Colomb et al., 2005), polymers (Colomb et al., 2002) and other inorganic materials (Tishko et al., 2012). This demonstrates the need of studies using this method for new applications viewing the biomedical field. Besides, in general, the main goal in the applications of DHM, considering the polarization or not, have been to describe methods of calculations of the DHM technique itself. In this study we intend to enlarge the scope of the application considering the specificities that should be kept in mind for a correct application of the DHM technique to biological sample.

In this chapter, is demonstrated a comparative study between image contrast of different types of biological samples using traditional optical microscopy techniques (OM) and the holographic techniques, with polarization (PHM) and the classical one (DHM), showing the

advantages of the holographic methods in visualization and analysis of microscopic structures. Besides, the staining influence in quality of phase and intensity image reconstruction is discussed. An additional study of birefringence and dichroism of anisotropic samples is developed in this chapter, using also traditional methods compared with the holographic polarization technique, being this study of major importance for the inner structure and composition analysis of a variety of biological objects.

2. Experimental set-up and methodology

In this work comparisons between the results obtained with classical techniques of optical microscopy and digital holographic microscopy are shown. In figure 1, the experimental set-up used in this work integrates both techniques.
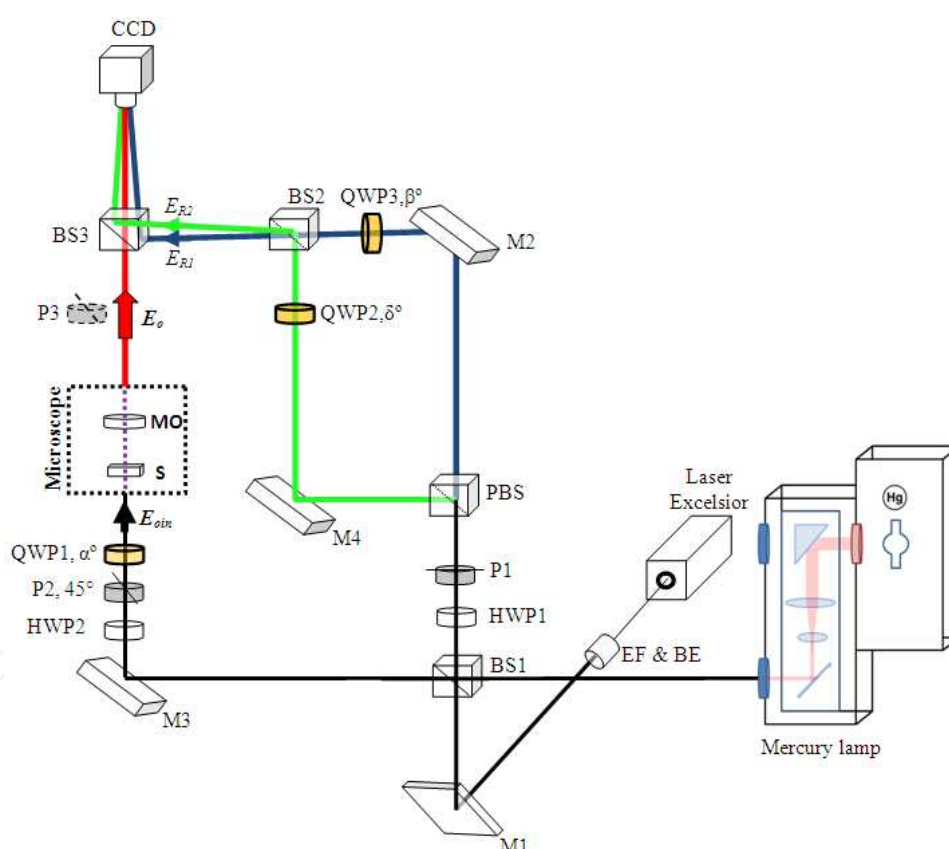

Figure 1. Experimental setup used in this work. In the next items are discussed the symbols.

The optical design allows the implementation of different classical techniques of optical microscopy and recording of single and polarization digital hologram. The same area of the sample is analyzed with classical techniques of optical microscopy using a mercury lamp as the light source. Single and polarization holograms are obtained with a solid state laser combined with an interferometric setup.

2.1. Classical techniques of optical microscopy

2.1.1. Differential polarization microscopy

Figure 2, shows optical setup for differential polarization microscopy (DPM).
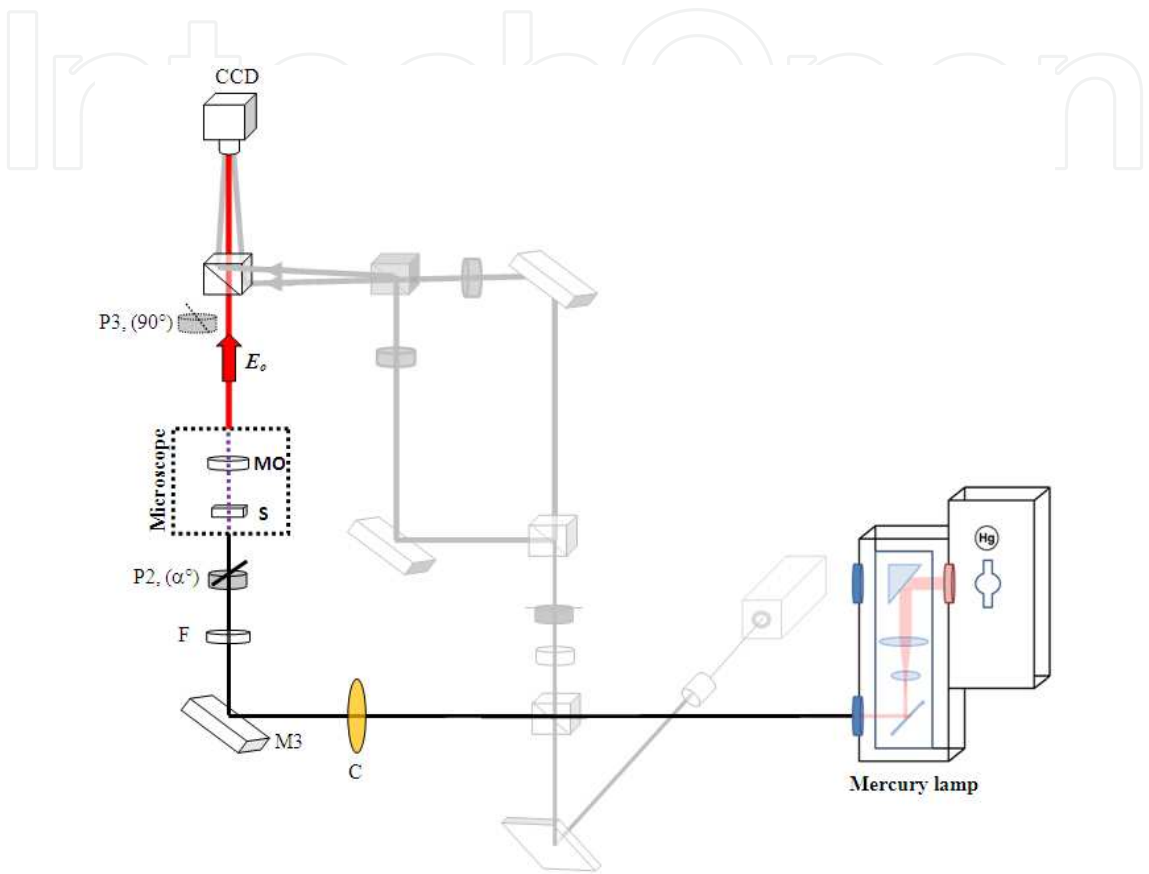
Figure 2. Differential Polarization Microscope. Light source is a mercury lamp, M3 is a mirror, C is the condenser system of the light beam, F is an interferential filter, P2 is a polarizer, S is the sample, MO is the objective lens and CCD is the digital capture device.

The dichroism images I_D can be reconstructed from the digital information. It is the quotient of the transmitted intensity difference by the sum of them,

$$I_D = \frac{I_{||} - I_{\perp}}{I_{||} + I_{\perp}}$$

(1)

$I_{||}$ is the intensity of the light beam polarized parallel to a reference direction α and $I_{\perp}$ is the intensity of the light beam polarized perpendicular to α.

To obtain information about orientation and and the average amount of aligned molecules, it is necessary to measure the ratio of the intensities transmitted with polarized perpendicular

to α, given in Eq. (1). Two linear differential images are used to perform the numerical image construction dependent of the molecule orientation.

2.1.2. Bright and polarization microscopy

Using the experimental setup of figure 2 the bright-field image is capture as the intensity of the light beam that crosses throughout the sample without using any polarizing element in light pathway. For polarization microscopy the polarizer P3 is inserted in the light path with orthogonal polarization with respect to the polarizer P2.

2.2. Digital holographic microscopy techniques

The Digital Holographic Microscopy has two steps to obtain the reconstructed wavefield, the recording and reconstruction of the digital hologram.

2.2.1. Recording of single digital hologram

Figure 3 shows the experimental set-up used for recording a single digital hologram. It is a Digital Holographic Microscope designed for transmission imaging with transparent sample.
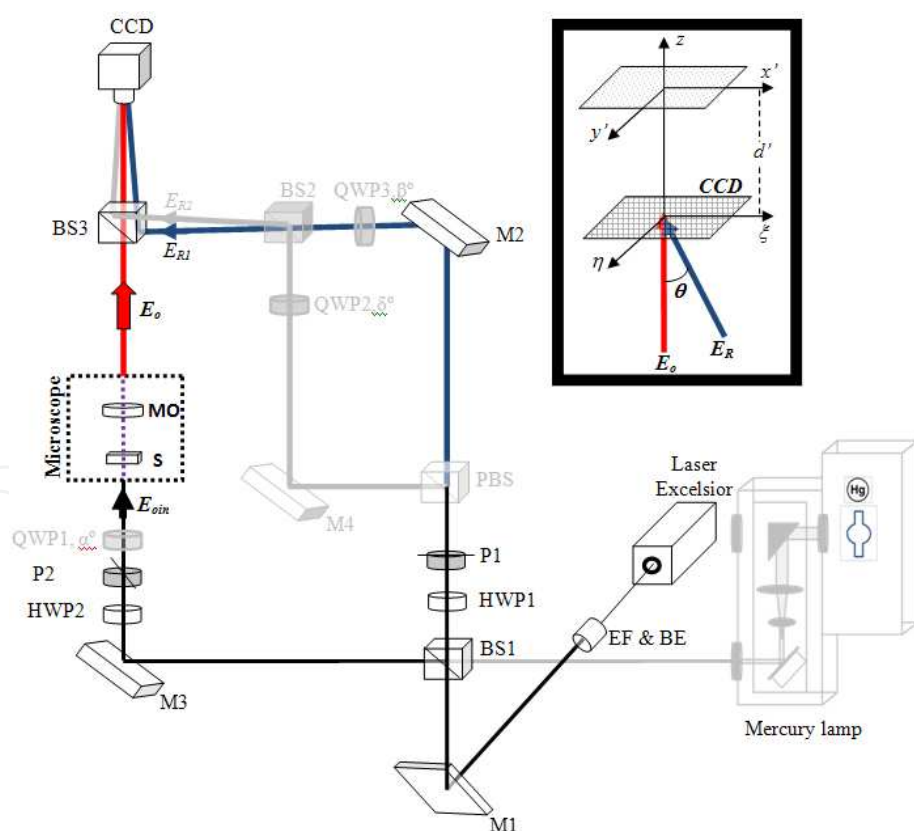
Figure 3. Experimental set-up: EF&BE, beam filter and expander; BS, beam splitter (the splitting ratio of BS1 and BS2 are 10/90 and 50/50 respectively); M, mirror; MO, microscope objective; S, sample; HWP, half wave plate; CCD, digital camera.

The basic architecture is that of a Mach-Zehnder interferometer. A linearly polarized solid state laser (Excelsior, λ=532 nm and 150 mW of power) is used as the light source. The expanded beam from the laser is divided by the beam splitter BS1 into reference and object beams. The microscope produces a magnified image of the object and the hologram plane is located between the microscope objective MO and the image plane $(x'-y')$ which is at a distance d' from the recording hologram plane $(\xi-\eta)$. In digital holographic microscopy we can consider the object wave emerging from the magnified image and not from the object itself (VanLigten & Osterberg, 1966).

With the combinations of the *HWP1, HWP2* and the polarizers *P1* and *P2* the intensities are adjusted in the reference arm and the object arm of the interferometer and the same polarization state is also guaranteed for both arms improving their interference. The specimen S is illuminated by a plane wave and a microscope objective, that produces a wave front called object wave E_o, collects the transmitted light. A condenser, not shown, is used to concentrate the light or focus the light in order that the entire beam passes into the MO, and in this case the wave front is spherical. At the exit of the interferometer the two beams are combined by beam splitter BS2 being formed at the CCD plane the interference pattern between the object wave E_o and the reference wave E_{R1}, which is recorded as the hologram of intensity $I_H(\xi,\eta)$,

$$I_H(\xi, \eta) = \mid E_o \mid^2 + \mid E_{R1} \mid^2 + E_{R1}^{*}{}^{*}E_o + E_{R1}E_o^{*} \tag{2}$$

where E_{R1}^{*} and E_o^{*} are the complex conjugates of the reference and object waves, respectively. The two first terms form the zero-order, the third and fourth terms are respectively the virtual (or conjugate image) and real image, which correspond to the interference terms. The off-axis geometry is considered; for this reason the mirror M2, which reflects the reference wave, is oriented so that the reference wave reaches the CCD camera with a small incidence angle with respect to the propagation direction of the object wave. A digital hologram is recorded by the CCD camera HDCE-10 with 1024x768 square pixels of size 4.65 μm, and transmitted to the computer by means of the IEEE 1394 interface. The digital hologram $I_H(j,l)$ is an array of $M \times N = 1024 \times 768$ 8-bit-encoded numbers that results from the two-dimensional sampling of $I_H(j,l)$ by the CCD camera,

$$I_H(j, l) = I_H(\xi, \eta)rect\left[\frac{\xi}{L_x}, \frac{\eta}{L_y}\right] \sum_{j=-M/2}^{M/2} \sum_{l=-N/2}^{N/2} \delta(\xi - j\varDelta\xi, \eta - l\varDelta\eta) \tag{3}$$

where j, l are integers defining the positions of the hologram pixels and $\varDelta\xi = \varDelta\eta = 4.65\ \mu m$ defines the sampling intervals in the hologram plane.

2.2.2. Recording of the polarization hologram

The experimental configuration for recording of polarization holograms is shown in figure 4. It is a Polarization Holographic Microscope (PHM) for the study of linear dichroism and birefringence of transparent samples.
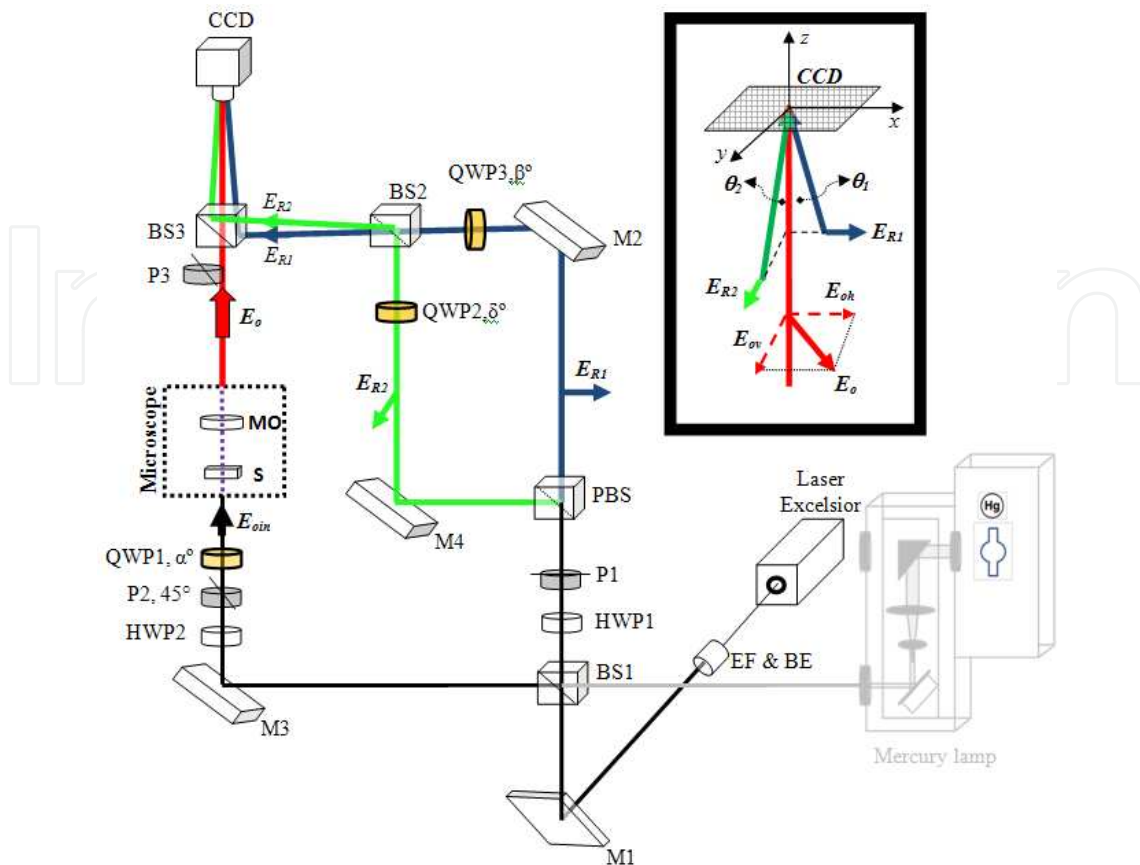
Figure 4. Schematic diagram of the Polarization Holographic Microscope for the study of linear dichroism and birefringence (symbology described in the text).

The experimental setup is composed by two *Mach-Zender* interferometers that form two reference beams E_{R1} and E_{R2}, with orthogonal polarization directions between each other, which interfere in the CCD camera with an object wave E_o in an off-axis geometry. As a light source a solid state laser with wavelenght of 532 nm and 150 mW of power is used. For samples that have some type of anisotropy, the state of polarization of the electric field E_o is different of the state of polarization of the incident electric field E_{oin}. The formation of the two reference waves in an architecture of a *Mach-Zender* interferometer ensures that these beams have the same optical path, becoming this an experimental novelty with respect to schemes reported in the literature. The polarized beam splitter (*PBS*) generates two beams with orthogonal states of polarization as reference waves; this orthogonality avoids any interference among then.

For studies of linear dichroism and birefringence, the polarizer *P2* imposes a 45° of polarization, with respect to reference wave polarization, to the E_{oin} wavefront that illuminates the object *S*. To maintain the linear polarization of the references waves E_{R1} and E_{R2} and incident electric field E_{oin} the fast axis of the quarter wave plates (QWP1, QWP2 and QWP3) are aligned parallel ($\alpha = \beta = \delta = 0^o$) with respect to the polarization states of the respective waves. For studies of circular dichroism and birefringence, over the sample, a circularly polarized light is incident. The polarization of the wave which illuminates the sample *S* is controlled by the quarter-wave plate *QWP1*, according to the waveplate's fast axis angle α relative to the polarizer transmission

axis *P2*: right-handed circular polarization (α = -45º), left-handed circular polarization (α = +45º). The two reference waves with orthogonal polarization are transmitted by the quarter-wave plates *QWP2* and *QWP2* with their fast axis forming angles of -45 ° and +45° with respect to the polarization states of the reference beams E_{R1} and E_{R2}. This configuration transforms the linear polarization of the reference waves E_{R1} and E_{R2} in right and left circular polarization, respectively. The two reference waves are directed by the beam splitter *BS3* to the *CCD* surface.

The light transmitted by the object is magnified by the microscopy objective *MO* producing an object wave E_o with orthogonal components E_{oh} and E_{ov} (detail in figure 4). The state of polarization of the object wave is different from that which illuminates the specimen E_{oin} and results in dichroism and birefringence properties of the specimen integrated along the propagation direction. The interference between the reference and object waves produces the polarization hologram. The hologram is recorded in an off-axis geometry with the three waves propagating along different directions. As shown in detail in figure 4, the object wave E_o has a normal incidence (along *Oz*) on the *Oxy* plane of the CCD. The reference waves E_{R1} and E_{R2} propagate symmetrically with respect to the plane *Oxz* with similar incidence angles θ_1 and θ_2, respectively. The angles of incidence θ_1 and θ_2 of the reference waves are controlled by the mirrors *M2* and *M4*; these mirrors are dielectric mirrors that do not change the state of polarization during the reference beams reflections. With the rotation of the two half wave plates *HWP1*, *HWP2* the reference wave intensities E_{R1}, E_{R2} and object wave E_o can be controlled.

With the polarization hologram reconstruction the polarization state of the wave object E_o can be calculated and thus represent the quantitative images of linear dichroism and birefringence. Capturing two polarization holograms, one with right circularly polarized light and the other with left circularly polarized light and then, reconstructing the polarization state of the beam emerging from the sample, the image of circular dichroism can be obtained comparing changes in the polarization state produced by variations when the circularly polarized light is rotated.

2.2.3. Formal description of polarization hologram formation

The intensity distribution of the hologram is described by the interference between E_o, E_{R1} and E_{R2}. As E_{R1} and E_{R2} have orthogonal polarization they do not interfere ($E_{R1} E_{R2}^{*} = E_{R1}^{*} E_{R2} = 0$). From the Jones formalism, the object wave E_o can be defined by the superposition of two fields E_{oh} and E_{ov} which have the same frequency and the same wave vector $\mathbf{k}_o$ along z, but with orthogonal vibration planes:

$$\mathbf{E}_O = \begin{pmatrix} E_{oh} \\ E_{ov} \\ 0 \end{pmatrix} \exp\left[i\left(k_o \hat{l} + \phi_O - \omega t\right)\right] = \begin{pmatrix} |E_O| \exp[i\phi_O] \\ |E_O| \exp[i\phi_O + \Delta\varphi_O] \\ 0 \end{pmatrix} \exp\left[i\left(k_o \hat{l} - \omega t\right)\right] \qquad (4)$$

where $\hat{l} = (\xi, \eta)$ is a position vector in the plane of the CCD, ϕ_o is the optical phase delay introduced by the specimen and experimented by the horizontally polarized wave and $\Delta\phi_o$ is the phase difference.

Similarly, the reference waves can be described by the relations,

$$E_{R1} = \begin{pmatrix} E_{R1} \\ 0 \\ 0 \end{pmatrix} \exp\left[i\left(k_1 \hat{l} - \omega t\right)\right]. \tag{5}$$

$$E_{R2} = \begin{pmatrix} 0 \\ E_{R2} \\ 0 \end{pmatrix} \exp\left[i\left(k_2 \hat{l} - \omega t\right)\right] \tag{6}$$

where k_o, k_1 and k_2 are the wave vectors:

$$k_o = \frac{2\pi}{\lambda} \begin{pmatrix} 0 \\ 0 \\ 1 \end{pmatrix}, k_1 = \frac{2\pi}{\lambda} \begin{pmatrix} 0 \\ sen(\theta_1) \\ \cos(\theta_1) \end{pmatrix}, k_o = \frac{2\pi}{\lambda} \begin{pmatrix} -sen(\theta_2) \\ 0 \\ \cos(\theta_2) \end{pmatrix} \tag{7}$$

On the interferometer exit, the interference between E_o, E_{R1} and E_{R2} creates the intensity distribution of the digital hologram, expressed by the equation,

$$
\begin{aligned}
I_H(\xi,\eta) &= \left(E_{R1} + E_{R2} + E_o\right)\left(E_{R1} + E_{R2} + E_o\right)^* \\
&= |E_{R1}|^2 + |E_{R2}|^2 + |E_o|^2 + E_{R1} E_o^* + E_{R2} E_o^* + E_{R1}^* E_o + E_{R2}^* E_o
\end{aligned} \tag{8}
$$

The first three terms in Eq. (8) form the zero order diffraction, the fourth and fifth terms produce two real images, corresponding to the horizontal and vertical component of the Jones vector. The last two terms produce the virtual images.

2.2.4. Polarization hologram reconstruction

The numerical reconstruction is realized with the D*ouble* P*ropagation* A*lgorithm* (Palacios et al., 2011). The intensity distribution $\psi(x',y',d')$ on the reconstruction plane (x',y') is obtained from the expression,

$$\psi(x',y',d') = \Im^{-1}\left\{ G \cdot \Im\left\{ I^f(\xi,\eta) \exp\left[\frac{i\pi}{\lambda D}(\xi^2 + \eta^2)\right]\right\} \exp\left(id'\sqrt{k^2 + k_u^2 + k_v^2}\right)\right\} \tag{9}$$

Where $G = A \exp[i\pi/\lambda D(u^2 + v^2)]$ denotes a constant phase factor, d' is the reconstruction distance, D is the distance among the CCD plane and the back focal plane of the objective lens, $\Im^{-1}$ is

the inverse Fourier Transform, $k=2\pi/\lambda$, k_u and k_v are the spatial frequencies corresponding respectively to u and v and $I^f(\xi, \eta)$ is the filtered hologram that contains only components of the real image.

Applying two spatial filters on the polarization hologram spectrum, the spatial frequencies components of the real image are selected separately. Calculating the inverse Fourier Transform of the spatial frequency components selected the two filtered and complex holograms, $H_h^f(\xi, \eta) = E_{R1}E_o^*$ and $H_v^f(\xi, \eta) = E_{R2}E_o^*$, can be obtained, corresponding respectively to the horizontal and vertical components of the Jones vector. Applying the numerical method of reconstruction to the holograms H_h^f and H_v^f the complex amplitudes distribution $\psi_h(x', y')$ and $\psi_v(x', y')$ in the reconstructed plane are obtained,

$$\psi_h(x',y',d') = \Im^{-1}\left\langle G\cdot\Im\left\{H_h^f(\xi,\eta)\exp\left[\frac{i\pi}{\lambda D}\left(\xi^2+\eta^2\right)\right]\right\}\exp\left(i\,d'\sqrt{k^2+k_u^2+k_v^2}\right)\right\rangle$$
$$\psi_v(x',y',d') = \Im^{-1}\left\langle G\cdot\Im\left\{H_v^f(\xi,\eta)\exp\left[\frac{i\pi}{\lambda D}\left(\xi^2+\eta^2\right)\right]\right\}\exp\left(i\,d'\sqrt{k^2+k_u^2+k_v^2}\right)\right\rangle$$

(10)

The fields $\psi_h(x', y')$ and $\psi_v(x', y')$ correspond to the orthogonal components of the object wave E_{oh} and E_{ov} respectively, therefore they can be represented as follows,

$$\psi_h(x',y') = \begin{pmatrix} I_{R1}(x',y')I_{oh}(x',y')\exp\left(i\left[\phi_h(x',y')-\phi_{R1}(x',y')\right]\right) \\ 0 \end{pmatrix}$$

(11)

and

$$\psi_v(x',y') = \begin{pmatrix} 0 \\ I_{R2}(x',y')I_{ov}(x',y')\exp\left(i\left[\phi_v(x',y')-\phi_{R2}(x',y')\right]\right) \end{pmatrix}$$

(12)

where I_{R1} and I_{R2} are the intensities of the reference waves; I_{ov} and I_{oh} are the intensities of the orthogonal components of the object beam E_o.

2.2.5. Determination of the parameters that characterizes the state of polarization

Making the intensities of the reference waves equal, $I_{R1}(x', y')=I_{R2}(x', y')$, (this is achieved adjusting the half-wave plates $HWP1$, $HWP2$, figure 4), the amplitude ratio β is calculated as,

$$\beta = \tan\left[\varepsilon(x',y')\right] = \frac{I_{oh}(x',y')}{I_{ov}(x',y')} = \frac{|\psi_h(x',y')|}{|\psi_v(x',y')|}$$

(13)

Moreover, the phase difference $\Delta\phi$ (x',y') between the orthogonal components of the object beam is calculated by,

$$\Delta\phi\left(x',y'\right)=\phi_h-\phi_v+\Delta\phi_R \tag{14}$$

where $\Delta\phi_R$ is the phase difference on the reference waves used to capture the hologram. Experimentally, this term is time dependent because of vibration and air flow, but this can be suppressed in the phase contrast image by a compensated phase difference $-\Delta\phi_R$. To adjust this phase displacement, is used an image area with known polarization. For that purpose, is inserted in the object beam a polarizer (*P3* in figure 4) oriented in such a way that produces a phase difference of 0 rad in the object beam area.

The corrected value of the phase difference $\Delta\phi_C(x',y')$ is obtained from,

$$\begin{aligned}\Delta\phi_C\left(x',y'\right)&=\Delta\phi\left(x',y'\right)+\Delta\phi_R\left(x',y'\right)=\phi_h\left(x',y'\right)-\phi_v\left(x',y'\right)\\&=\arg\left[\psi_h\left(x',y'\right)\right]-\arg\left[\psi_v\left(x',y'\right)\right]\end{aligned} \tag{15}$$

If the parameters "**β**" and "$\Delta\phi$" are experimentally measured, then the modification of the polarization state of the wave transmitted through the specimen is correlated to its structure, composition and optical properties. There are two physical phenomena that can change the polarization state: the **dichroism** and the **birefringence**.

a. **Dichroism**: Several crystalline materials absorb more light at an incident plane of polarization than at another plane, thus as the light travels through the material, its polarization state changes. This absorption anisotropy is called dichroism. The evaluation of the linear dichroism property of a specimen can be made by calculating the ratio of amplitudes of the orthogonal components of the light passing through the specimen.

b. **Birefringence**: Birefringence is a property of materials with refractive index anisotropy. After the polarized light crosses a birefringent sample, there is a relative phase change on the two field components and the beam resulted from the interference of the two wave fields is generally elliptically polarized, i.e. this property can be described through the phase difference in the orthogonal components of light crossing the specimen.

3. Verification of the experimental setup

3.1. Obtainment of the phase contrast image

The verification of the experimental setup of DHM was obtained by processing holograms of an object with well-known parameters. The calibration of the DHM setup in XY dimensions was performed by using USA Airforce standard (USAF 1951). The vertical calibration along Z-axis is intrinsically linked to the phase measurements. Overall performance of DHM was

checked using polystyrene beads with refractive index $n_o = 1.59$. Diluted beads suspension in water was put onto a microscopic slide and dried. A drop of glycerol-based mounting media with refractive index of 1.46 was layered up and the slide covered with a glass coverslip. Results of DHM are shown in figure 5.


(a)   (b)
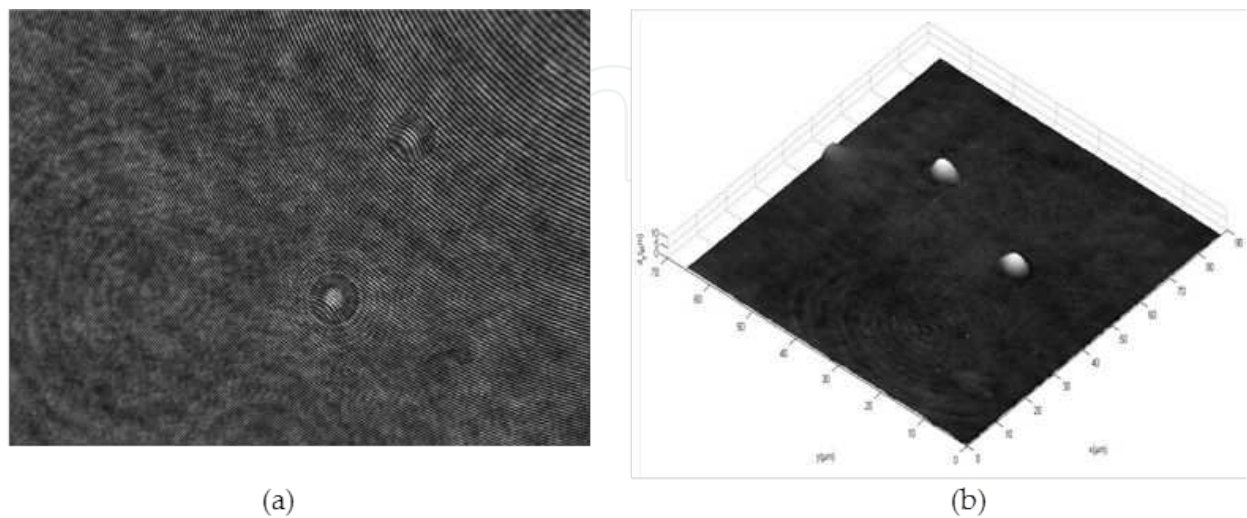
Figure 5. (a) Digital hologram of polystyrene spheres. (b) Phase contrast image reconstruction

The calculated averaged XYZ bead diameter of 6.42 µm is very close to the manufacturer data.

3.2. Measurement of the polarization states

For obtaining the polarization states is used as sample a $\lambda/4$ plate to generate a variety of polarization states of the object wave, see figure 6. The object was placed at a distance of 170 mm from the surface of the CCD. The wave incident on the object is linearly polarized with the polarizer *P2* with an orientation of 45° with respect to the horizontal axis. The polarization state of the light wave transmitted by the $\lambda/4$ plate was analyzed for several orientations α (angle between the fast axis of the quarter-wave plate and transmission axis of the polarizer *P2*) between 0° and 90 ° with a 3° shifts.
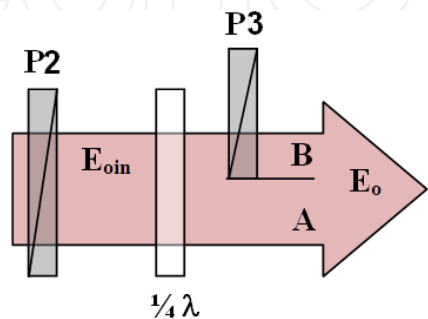

Figure 6. Object arm diagram for PHM experimental setup validation. E_{oin}, illuminating wave; E_o, object wave; polarizer P3 has the transmission axis parallel to that of polarizer P2; B is the reference area, where the phase difference is zero, and A is the area for analysis.

The polarizer $P3$ oriented at an angle $\delta = 45°$ is used as reference area for determining phase difference of compensation. The area B is the reference where the phase difference is zero and A is the area for analysis. The calculated mean value in the area B is used as compensation value $\Delta\phi_R$.

Figure 7a shows the polarization digital hologram of the $\lambda/4$ plate with $\alpha = 0°$. In figure 7b and 7c is shown, respectively, the reconstruction of the amplitude ratio and phase difference images. The orientation of the polarizer $P3$ is $\delta = 45°$. The area B in figure 7b shows the reference area determined by the polarizer $P3$ in figure 6 and area A shows the area of the examined plate.

(a)   (b)   (c)
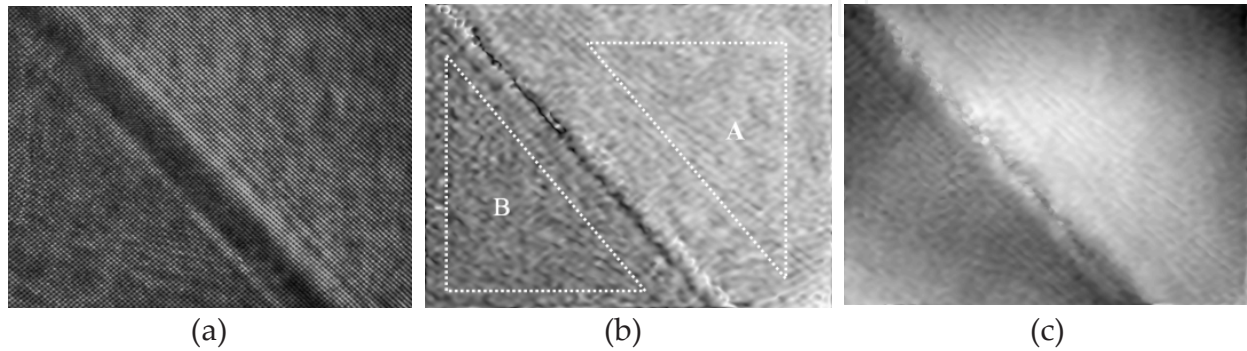
Figure 7. (a) Polarization hologram. Calculated (b) amplitude ratio, β and (c) phase difference $\Delta\phi_C$ for the quarter wave plate ($\frac{1}{4}\lambda$ in figure 6) with the orientation of $\alpha = 0°$ respect to the polarizer transmission axis $P2$ in figure 6. Area A is for analysis ($\frac{1}{4}\lambda$) and area B is for the reference (P3 in figure 6).

Figure 8a and 8b show, respectively, the amplitude ratio β and the corrected phase difference $\Delta\phi_C$. The mean value obtained in area A is used as the representative experimental value on the graphic (filled circles).

Using the expressions $\gamma = \frac{1}{2} atan[\tan(2atan(\beta))\cos(\Delta\phi)]$ and $\omega = \frac{1}{2} asin[\sin(2atan(\beta))\sin(\Delta\phi)]$ there were determined the azimuth γ values, figure 8c, and the deformation of the ellipse ω, figure 8d. The theoretical values calculation for β, $\Delta\phi_c$, γ and ω (continuous curve) were obtained by the following reasoning: the polarization state of the object beam $\psi_T(x,y)$ which emerges from the $\lambda/4$ plate is theoretically calculated by the product of the $\frac{1}{4}\lambda$ plate Jones matrix and the Jones vector of the incident wave linearly polarized with an orientation of 45°,

$$\psi_T(x,y) = \begin{pmatrix} \psi_{Th}(x,y) \\ \psi_{Tv}(x,y) \end{pmatrix}$$
$$= \begin{pmatrix} \cos\alpha & -sen\,\alpha \\ sen\,\alpha & \cos\alpha \end{pmatrix} \begin{bmatrix} \exp(i\Delta) & 0 \\ 0 & \exp(-i\Delta) \end{bmatrix} \times \begin{pmatrix} \cos\alpha & sen\,\alpha \\ -sen\,\alpha & \cos\alpha \end{pmatrix} \begin{pmatrix} 1 \\ 1 \end{pmatrix} \tag{16}$$

where $\Delta = \pi/4$ is the phase difference between the orthogonal components of the wave emerging from the $\frac{1}{4}\lambda$ plate. The theoretical values of the ratio of amplitudes β and the phase differences
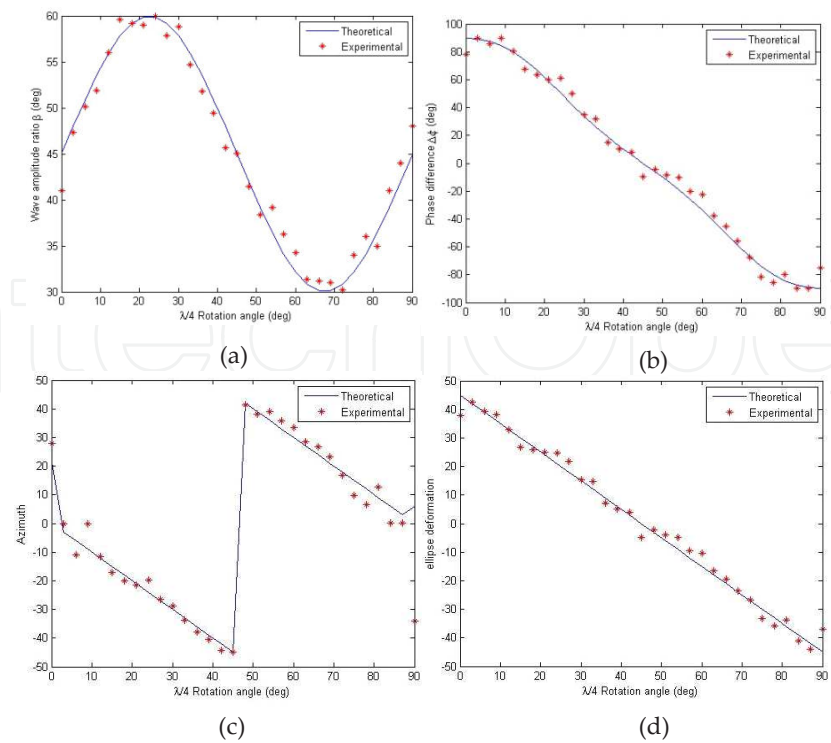
Figure 8. Filled circles) experimental values of (a) amplitude ratio, (b) phase difference (c) azimuth and (d) ellipse deformation of the wave transmitted by the λ/4 plate. (Continuous curve) theoretical values.

$\Delta\phi_C$ were calculated directly by substituting Eq. (16) into Eq. (13) and Eq. (15) respectively. From figure 8, it can be noted that the experimental values are in good agreement with the theoretical values; this ensures the implementation of the designed setup to study objects with distinctive optical activity.

4. Phase contrast method

In this section are presented the results of Digital Holographic Microscopy (DHM) applied to the analysis of different types of biological samples. The advantages of DHM upon bright-field optical microscopy (OM) in visualization and analysis of microscopic structures are illustrated and discussed.

The DHM adds information to the conventional microscopic morphology of isolated cells, obtained either from clinical and research specimens or from cell cultures. Fixative substances and stains were not required, nor essential. Nevertheless, stains were very convenient tools and added some information when conventional morphology and MHD images were considered not equivalent. In general, stained slides analysis succeeded well for three-dimensional image reconstruction of known samples, even if the main Cytology and Histology stains are intended to discriminate structures only through light intensity modification, while light phase effects are not valued or are even minimized by the technical protocols. Then, except for some

particular samples, stains were not of help in increasing the quality of the reconstructed phase images, and staining artifacts were not considered relevant to quantitative phase analysis. Blood smears or body fluid cells prepared by cytocentrifugation or sedimentation techniques were air dried before being dehydrated with methanol for fixation and stained with Hematological stains (Leishmann, Rosenfeld) with good results. Papanicolaou and Hematoxylin-Eosin (HE) staining procedures were also assayed. As for any microscopic technique, correct fixation and staining procedures were relevant to assure good quality morphology, the technical quality stringency being essentially equivalent for bright field analysis and for MHD. Fixative preserved samples, unstained or only slightly stained consistently gave superior results for phase image reconstruction by the MHD technique than the brilliant and deeply stained samples. Unpreserved and labile fresh specimens stained or not could also be observed. Mounting media changes could evince or veil sample morphology, then mounting media composition and physical properties was carefully considered when phase contrast images were obtained from samples prepared with glycerol, resins or Permount.

The reconstructed topographic profile was determined by the actual expected specimen dimensions, but was also modified by the intrinsic composition of each structure, as can be easily realized in comparing the MHD image of macrophage and lymphocytes in the figure 9. The phase images reconstruction of the cells of rat peritoneal fluid (figure 9) was obtained after an isosmotic PBS wash procedure in a normal and otherwise unmanipulated adult animal. The resulting cell suspension was cytocentrifuged over a glass slide, fixed with methanol and stained with Rosenfeld stain (Eosin/Methylene Blue/Methylene Azures). No mounting media was employed.

(a) (b)
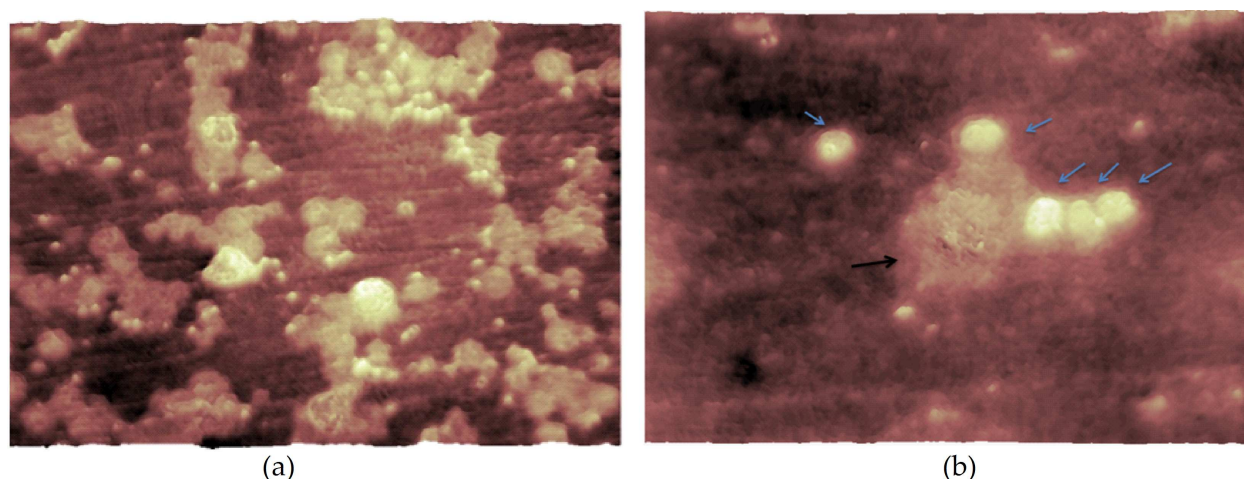
Figure 9. Rat peritoneal fluid cells obtained after phosphate buffered saline (PBS) flux of the peritoneal cavity, Rosenfeld stain. Slide provided by the researcher Dalila Cunha de Oliveira, from the archives of her graduate student Master Thesis tutored by Dr. Ricardo Ambrosio Foch, (FCF-USP Ethical Committee Protocol number 316/2011). Phase image reconstructions with DHM. Magnification (A) 10x objective, (B) 40x objective.

When low magnification was used, the discrimination of the contours of the distinct cells in the reconstructed image presented some difficulties, as seen in the figure 9-A. Peritoneal fluid lipoproteins and other methanol insoluble molecules produced some background depth

fluctuation in the phase reconstructed image. Observed in a greater magnification, as in figure 9-B, the different cells were more clearly defined, showing color intensities proportional to their relative contributions of the refractive index magnitudes and the thickness of the sample structural components. In figure 9-B lymphocytes are presented with light arrows and the monocyte/macrophage with dark arrow. The peculiarities about the topography of the monocyte/macrophage and lymphocyte cells well express how their structural differences, besides their expected dimensions, contribute to the reconstruted image. The dense chromatin and the protein rich cytoplasm of the lymphocytes contributed to produce a bright yellow color, while the lose chromatin and the foamy microvacuolated cytoplasm of the macrophages produced darker orange-brown color.

(a)   (b)

(c)   (d)
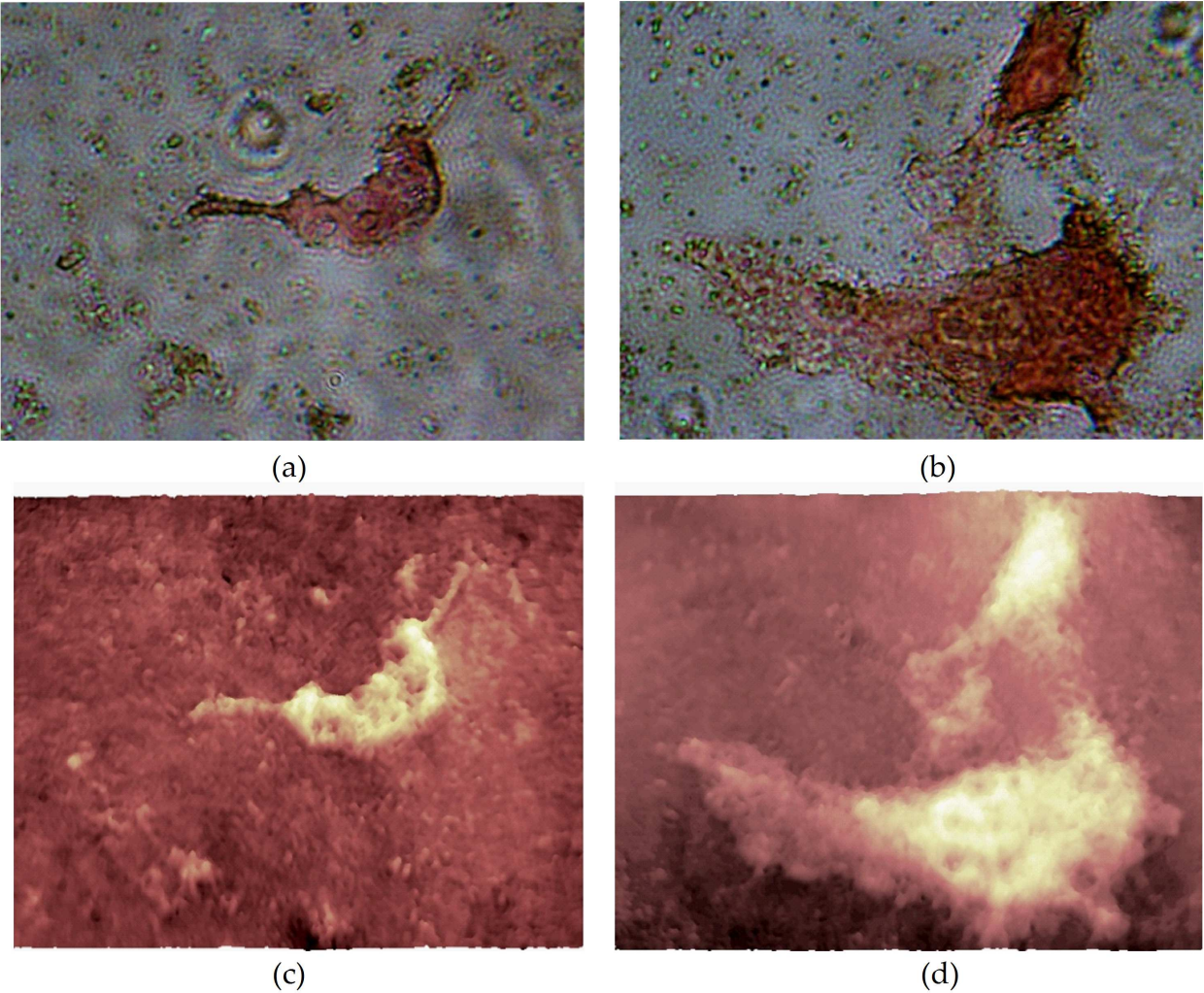
Figure 10. Fibroblast cells of FN1 cell line kindly furnished by Dr. Durvanei Augusto Maria were cultivated by Dr. Sonia E. Will over round coverslides and stained with Picrosirius Red for collagen. (A, B) Optical microscopy images. (C, D) Phase contrast images reconstructed with DHM. Magnification 10x objective.

Syrius Red staining for collagen fibers was used to evaluate MHR performance in the study of extracellular matrix structures and fibroblast physiology. Figure 10A and 10B show the optical microscopy images. Figure 10C and 10D show the phase contrast images of fibroblast
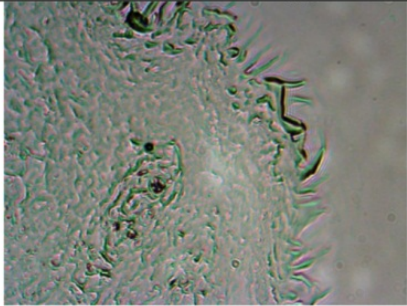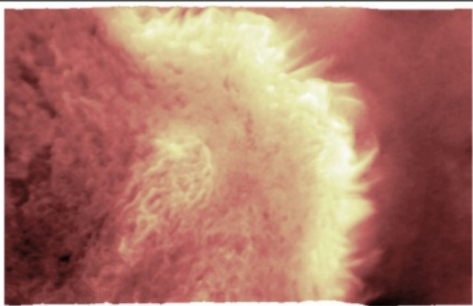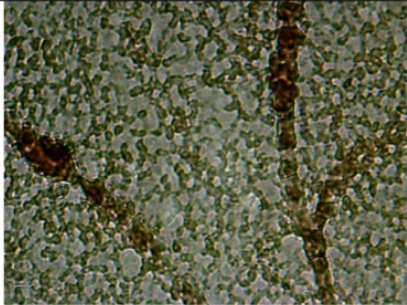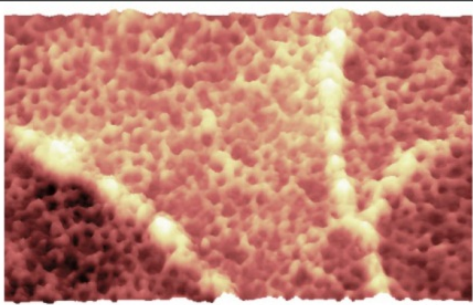
cells stained with the picrosyrius technique (Junqueira et al., 1979). Phase contrast image reconstructed with DHM and bright-filed image under mercury lamp illumination was obtained from the same area of the sample, both are shown for comparison.

As shown in figures 10-C and 10-D the cells structures and the fibers produced by them are better differentiated by means of difference in phase values of each one.

Digital Holographic Microscopy showed suitable for unstained tissue observation. Even unstained sections of paraffin embedded tissues could reveal more details about topography and composition of the samples than did bright field optical microscopy. Archive samples were not destroyed through the observation by the technique and the sample could be subsequently prepared for special molecular biology based on immunological staining procedures, when convenient.
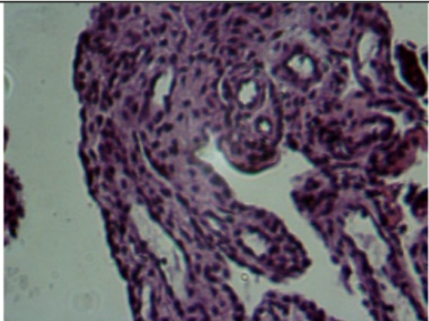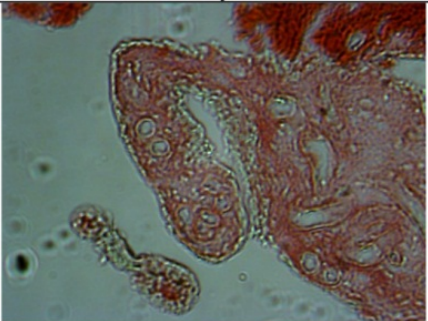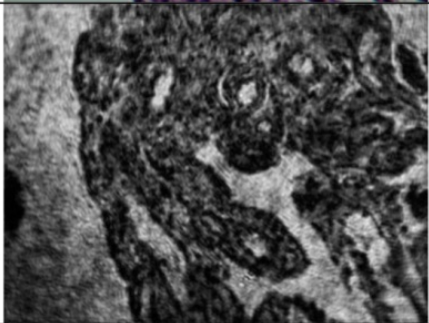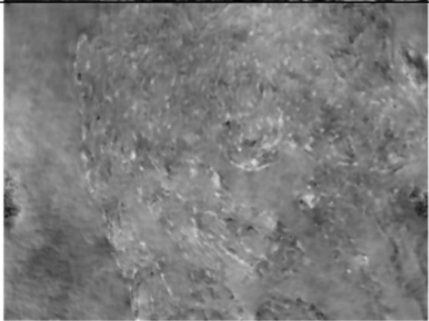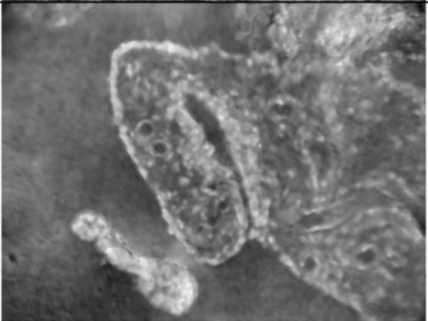
Figure 11 shows an example of this kind of material, from the personal archive of Dr. Bruno Gomes Vasconcelos, in which the structural information on the gustative epithelia could be observed in the paraffin embedded section of the tongue tissue sample, figure 11A-B. On the other hand, fresh and unfixed tissue samples could also be studied. Microcirculation of the chorioallantoic membrane of the chicken embryo (CAM) furnished an example about the possibilities of analysis of capillary mesh structure, applicable to the study of the microcirculation of tissues, figure 11C-D.

Figure 11. (A,B) Histological section of *Cavia porcellus* tongue, Fixation in formaldehyde 10%, embedding in paraffin, cut of 5 µm, stained with HE, magnification of 10x. (C,D) Chicken embryo chorioallantoic membrane distended over glass slides and analysed previously to fixative procedures showing good preservation of the capillary mesh. (FCF-USP Ethical committee protocol no. 274/2010).

White eggs of *Gallus domesticus*, (Granja Hyline) were incubated for 10days in an automatic incubator thermostated (Zagas) at 37.2 º C, relative humidity 50%, with periodical turns at two hour intervals. CAM sampling was carried during the 10th day of incubation, after the eggs were placed for at least 30 min at 4°C before being opened. The shells were cut in the air chamber and the CAM was collected and distended over glass slides for vasculature analysis as previously described (Will et al, 2011). Samples of chorioallantoic membrane could be analyzed previously to fixative procedures showing good preservation of the capillary mesh. (Ethical committee protocol no. 274/2010).

The biochemical composition of the main analyzed structures, the red color of hemoglobin and the fiber rich vasculature ease the direct observation of the unstained specimens. The phase contrast images, reconstructed by DHM, provide an accurate visualization of three-dimensional structures of the sample, in addition provide a quantitative assessment of the refractive index and thickness of the sample that ensure the indirect calculation of specimen intrinsic parameters.

Type of image	HE	Picrosyrius
Optical Microscopy		
Intensity Images		
Phase contrast images		

Figure 12. Glass slides with equine dissecating osteochondritis (OCD) synovial membrane material. HE and Picrosyrius stainings, 10x objective. Permount mount. Clinical samples kindly furnished by Aline Ambrogi Franco Prado (FMVZ-USP Ethical Commitee protocol no. 2771/2012)

4.1. Influence of staining and mounting procedures

The effect of sample preparation on the quality of phase and intensity image reconstructions is presented in figure 12. The results of Synovial Membrane samples were obtained using two different staining sorts. The images obtained with optical microscopy display high contrast with the two staining sorts, although the staining influences the contrast quality in the two types of images observed with DHM. Thus, in the case of HE stain it intensifies the contrast of the intensity reconstructed image and decreases it in the phase contrast image. An opposite effect is observed when the Picrosyrius stain is used. This effect was ascribed to the Permount mounting associated to the optimal intensity contrast enhancing staining procedure obtained with HE technique, which relies on the base of its universal and general preference use for routine histological samples. The Picrosirius stain sets for collagen fibers demonstration, and collagen demonstrated to produce good phase image reconstructs, superimposed to Picrosirius stained regions as could be demonstrated below.

5. Polarization contrast method

An orderly material can be selectively detected in the presence of random absorbent. Thus, orderly structures can be detected and quantified and their orientation can be stated in complex objects. The selectivity depends on the polarization direct relation with the chromophores extinction coefficient.

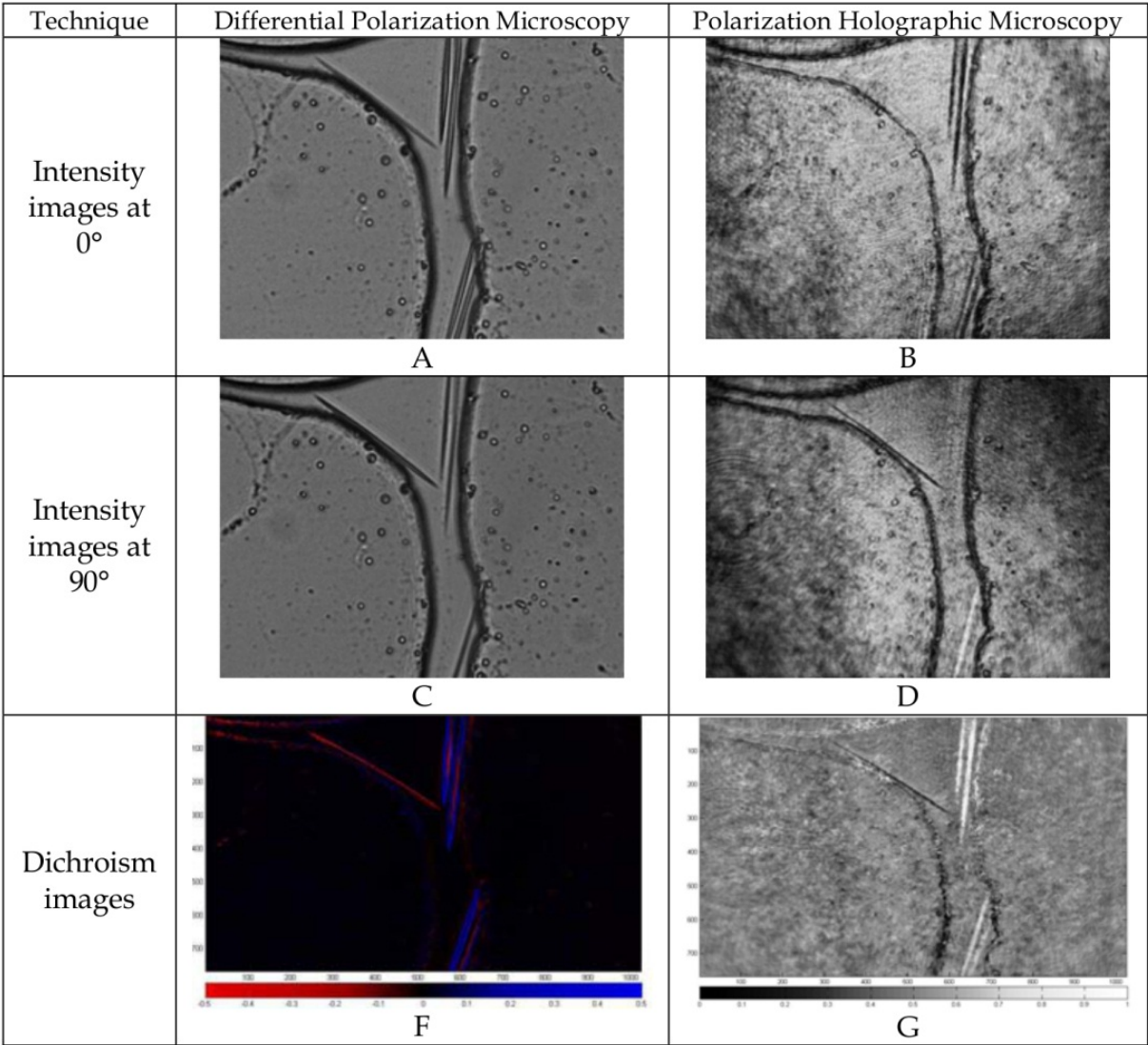### 5.1. Visualization of linear dichroism in *Calcium Oxalate*

Figure 13 shows the visualization of linear dichroism in *Calcium Oxalate* sample extracted from *Sansevieria trifasciata* sap.

From figure 13, is possible to compare the results of the dichroism image reconstruction obtained with DPM and PHM. Difference in the intensity images obtained with specific polarization states of the object beam for each technique is possible to notice. The holographic images show a higher contrast for the calcium oxalate samples when compared with those obtained by the traditional method. The dichroism image obtained by the Differential Microscopy, is represented by a color bar distributed between blue and red shades, being the red shades referring to negative dichroism and the blue referring to positive dichroism. Differently, the dichroism image obtained with the holographic method is shown in gray scale, where the lighter shades correspond to positive dichroism values and the dark shades represent negative dichroism values. When these two images are compared is possible to see a correspondence among these images.

5.2. Cell death through dye induced optical activity

Figure 14-A presents optical microscope image of an endothelial cell sample where the presence of undesirable objects (such as air bubbles or particulate material) do not guarantee

| Technique	Differential Polarization Microscopy	Polarization Holographic Microscopy
Intensity images at 0°	A	B
Intensity images at 90°	C	D
Dichroism images	F	G

Figure 13. Visualization of linear dichroism in *Calcium Oxalate* sample extracted from *Sansevieria trifasciata* sap. (A,C) Intensity images obtained with polarizer (*P2* in figure 4) oriented at 0° and 90° with the Differential Polarization Microscopy. (B,D) reconstructed intensity image with the Polarization Holographic Microscopy. (F,G) dichroism image reconstruction obtained with Eq. (1) and Eq. (13) respectivelly.

a good visualization of the cells. The phase contrast image (Figure 14-B) obtained with holographic microscopy, still retains the undesirable objects reconstruction.

When the Polarization Holographic Microscopy is used, the possibility of staining (*Picrosirius Red for collagen fibers*) to introduce optical activity in the sample allows a more differentiated study of the cells. Reconstructing the Polarization Digital Hologram, Fig. 14-C, are reconstructed the molecular alignment structure generating birefringence or dichroism, without showing other types of structures, Figure 14-D. Some of these are not displayed in the optical microscopy image. Besides improving the internal structure organization of cell visualization, the Polarization Holographic Microscopy allows observing the molecular alignment within
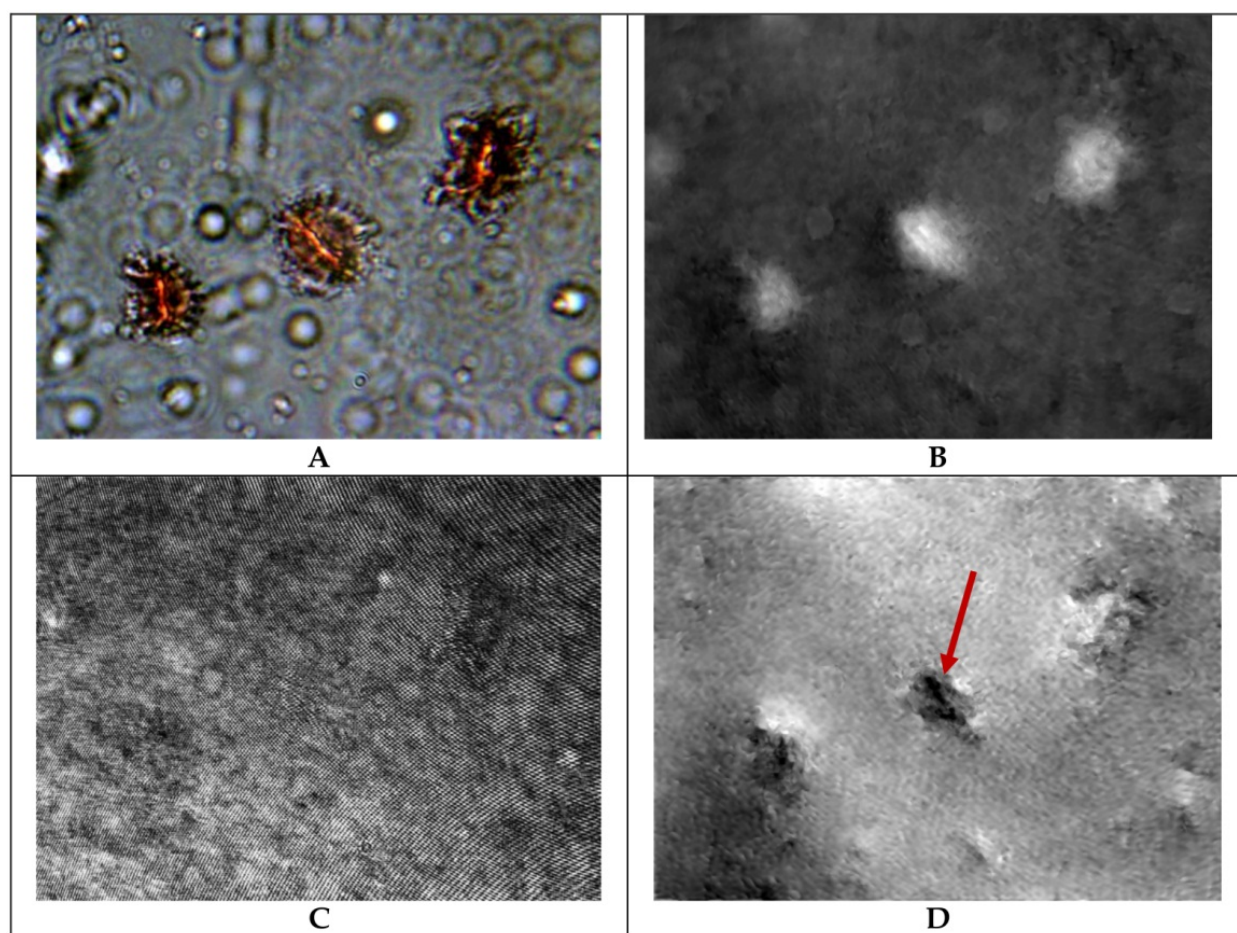
Figure 14. Cell death visualization by polarization staining in the presence of particulates and air bubbles. HUVEC cells (kindly furnished by Dr. Durvanei Augusto Maria) induced to cell death by silver nanoparticles exposure i*n vitro* (22ppm, nanosilver Khemia)*,* Picrosyrius stain. (A) Optical microscopy image, (B) Phase contrast image, (C) Polarization hologram (D) Polarization hologram reconstruction. Magnification 10x objective.

the cell. This molecular alignment is well observed in the signed cell with an arrow in Figure 14-D. In this cell, the molecular alignment is most evidently displayed because of their vitality, which is not shown on the less vital neighboring cells.

5.3. Visualization of birefringence in metronidazole

The Polarization Holographic Microscopy is suitable for crystalline and amorphous powder analysis. The sample and mounting media optical properties must be considered, as well as aggregation interference. In the figure 15 it is presented the result of a metronidazole sample processing. The optical microscopy image, figure 15-A, shows the intensity changes in light passing through the sample. The use of holographic microscopy enables to quantify the topographic characteristics the of the powder grains through the phase image reconstruction (figure 15-B) knowing that the metronidazole refractive index is n_o = *1.618* and the medium immersion (glycerol) refractive index is n_m=*1.437.*
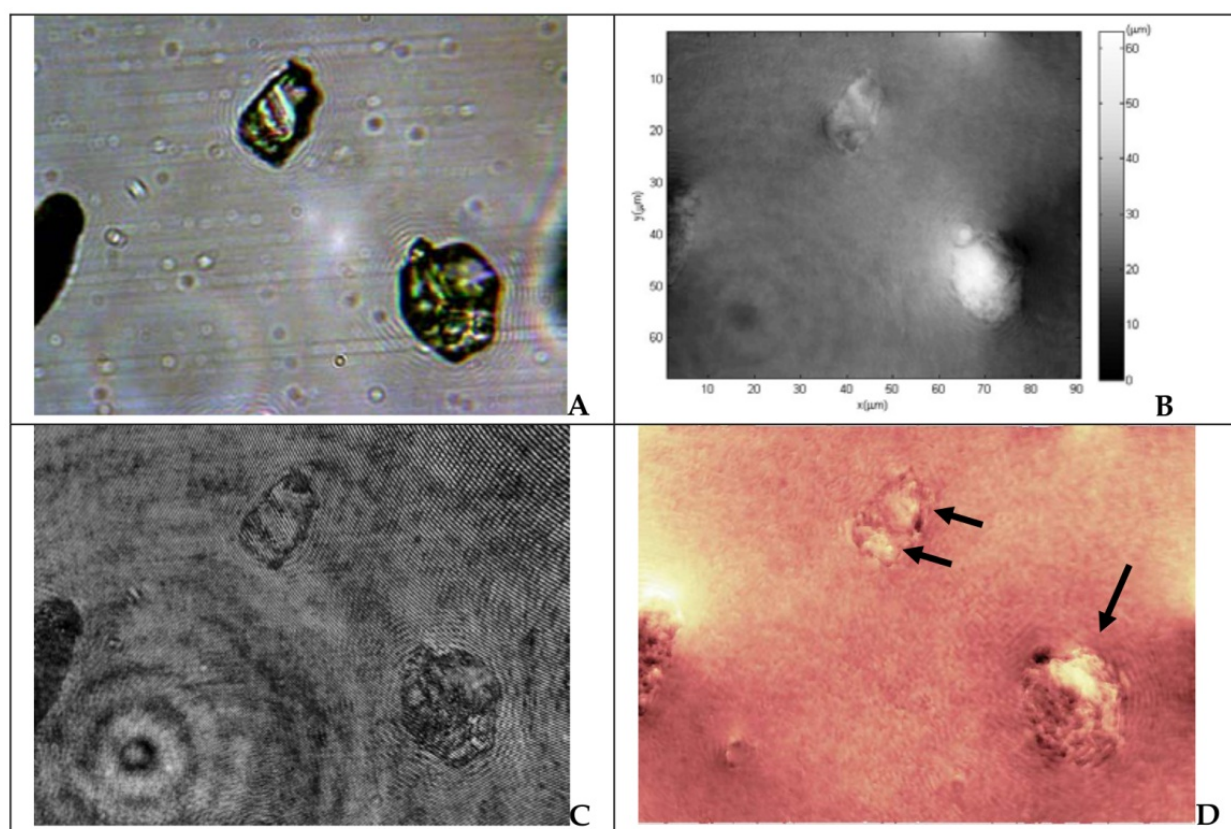
Figure 15. Metronidazole powder material observed in glycerol suspension. Thin film produced by placing a suspension drop between 1mm thick glassslide and 00 coverslip, 10x objective. (A) Optical microscopy image, (B) Phase contrast image obtained with single hologram reconstruction, (C) Polarization hologram, (D) Polarization hologram reconstruction where is observed the linear birefringence of this drug. Sample kindly provided by the researcher Michele Georges Issa, Master degree graduate student tutored by Dr. Humberto Ferraz.

The polarization hologram reconstruction (figure 15-C), reveal the lineal birefringence characteristics from this drug by evidenciating the chemical crystals alignment which comprises the metronidazole structure, figure 15-D (dark arrows).

6. Conclusion

In this chapter were discussed the phase and polarization contrast methods for digital holographic microscopy. Both contrast methods were applied to different types of biological samples. The potentialities of DHM were shown through the comparison with classical techniques of optical microscopy. It was evidenced that the DHM offers a more precise visualization of the structures that compose the samples as well as others characteristics obtained by means of the phase contrast image analysis that contains information about the refractive index and thickness in each portion of the specimen. The effect of sample preparation in the quality of phase and amplitude images reconstruction was shown. There were analyzed different types of biological samples that include different types of tissues, cellular culture,

drugs and the Chicken embryo chorioallantoic membrane. The possibilities of the DHM for obtaining the polarization state of the samples were also shown. It was demonstrated that the knowledge of the polarization state allows a wider characterization of the sample, such as the visualization of linear dichroism and birefringence, cell differentiation through special components or dye induced optical activity. It was demonstrated that the use of polarization holographic microscopy provides not only high specificity for the detection of ordered structures, but also for cellular vitality status.

Acknowledgements

Author details

Francisco Palacios[1], Oneida Font[2], Guillermo Palacios[1], Jorge Ricardo[1], Miriela Escobedo[1], Ligia Ferreira Gomes[2], Isis Vasconcelos[2], Mikiya Muramatsu[2], Diogo Soga[2], Aline Prado[2] and Valin José[3]

1 University of Oriente, Cuba

2 University of Sao Paulo, Brazil

3 Polytechnic Institute "José A. Echeverría", Cuba

References

[1] Buraga-Lefebre, C.; Coetmellec, S.; Lebrun D.; & Ozkul C. (2000). Opt. Laser Eng. 33, 409.

[2] Carl, D.; Kemper, B.; Wernicke, G. & Von Bally, G. (2004). Appl. Opt. 43, pp. 6536-6544.

[3] Colomb, T.; Dahlgren, P.; Beghuin, D.; Cuche, E.; Marquet, P. & Depeursinge C. (2002). Appl. Opt. 41, 27–37.

[4] Colomb, T.; Cuche, E.; Montfort, F.; Marquet, P.; & Depeursinge C. (2004). Opt. Commun. 231, 137–147.

[5] Colomb, T.; Dahlgren, P.; Beghuin, D.; Cuche, E.; Marquet, P. & Depeursinge, C. (2002). Appl. Opt., Vol. 41, No. 1, pp.27-37.

[6] Cuche, E.; Bevilacqua, F. & Depeursinge, C. (1999). Opt. Lett. Vol. 24, pp.291-293.

[7] Emery, Y.; Cuche, E.; Colomb, T.; Depeursinge, C.; Rappaz, B.; Marquet, P. & Magistretti, P. (2007). J. of Phys.: Conf. Series 61 (1) , 1317-1321.

[8] Hu, C.; Zhong, J.; Weng, J. & Yan, G. (2011). Proceedings of the ISBB, pp.271-274, doi: 10.1109/ISBB.2011.6107699.

[9] Junqueira, L.; Bignolas, G. & Brentani, R. (1979). Histochem J 11:447–455.

[10] Kemper, B.; Carl, D.; Höink, A.; Von Bally, G.; Bredebusch, I. & Schnekenburger, J. (2006). Proceeding of SPIE, 6191.

[11] Kim, M. (2010). J. Opt. Soc. Korea, Vol. 14, No. 2, pp. 77-89.

[12] Nomarski, G. (1955). J. Phys. Radium 16, 9.

[13] Nomura, T.; Javidi, B.; Murata, S.; Nitanai, E. & Numata T. (2007). Opt. Lett. 32, 481–483.

[14] Palacios, F.; Ricardo, J.;Palacios, D.; Gonçalves, E.;Valin, J. & De Souza, R. (2005). Opt. Commun. 248 41.

[15] Palacios, F.; Font O.; Ricardo, J.; Palacios, G.; Muramatsu M.; Soga, D.; Palacios, D. & Monroy, F.; (2011). Advanced Holography - Metrology and Imaging, Ed. InTech, ISBN 978-953-307-729-1, Chap. 9, pp. 183-206.

[16] Pavillon, N.; Kuhn, J.; Moratal, C.; Jourdain, P. & Depeursinge, C. (2012). PLoS ONE, Vol. 7, No.1, e30912. doi:10.1371/journal.pone.0030912.

[17] Popescu, G.; Deflores, L.; Vaughan, J.; Badizadegan, K.; Iwai, H.; Dasari, R. & Feld, M. (2004). Opt. Lett. 29, pp. 2503-2505.

[18] Pluta, M. (1988). Opt. Laser Techn. 20 (2), 81-88

[19] Ricardo, J.; Muramatsu, M.; Palacios, F.; Gesualdi, M.; Font, O; Valin, J.; Escobedo, M.; Herold, S.; Palacios, D.; Palacios, G. & Sánchez, A. (2011). J. Phys. Conf. Ser. 274, 012066 doi: 10.1088/1742-6596/274/1/012066.

[20] Seebacher, S.; Osten, W.; Baumbach, T. & Jüptner W. (2001). Opt. Laser Eng. 36, 103.

[21] Schilling, B.; Poom, T.; Indebetouw, G.; Storrie, B.; Shinoda, K.; Suzuki, Y.; & Wu, M. (1997). Opt. Lett. 22 1506.

[22] Tishko, T.; Tishko , D. & Titar, V. (2012). J. Opt. Techn. 79 (6), 340-343.

[23] VanLigten, R. F. & Osterberg, H. (1966). Nature, 211, pp. 282-283.

[24] Wang, Z.; Millet, L.; Gillette, M. & Popescu, G. (2008). Opt. Lett., Vol. 33, No. 11, pp. 1270-1272.

[25] Xu, W.; Jericho, M.; Meinertzhagen, I. & Kreuser, H. (2001). Cell Biol. 20, 301.

[26] Zernike, F. (1942). Physica 9, 686.

[27] Zernike, F. (1942). Physica 9, 974.